Buckling and Vibration of Externally Pressurized Conical Shells with Continuous and Discontinuous Rings

Milton H. Schneider Jr.,* Richard F. Snell,† John J. Tracy,‡ and Daniel R. Powers§
McDonnell Douglas Space Systems Company, Huntington Beach, California 92647

External pressure buckling, free vibration, and external pressure–vibration interaction data were obtained on a sixth scale Lexan model of the Titan IV (prototype) nose cone fairing. The objectives of these experiments were to validate analytical models used in the prototype design and to provide experimental data on the effects of discontinuous circumferential rings, flexible ring-to-shell attachment, separation rails, and skin splices. In addition, a nondestructive buckling load predictive test technique based on natural frequencies was evaluated using the Lexan model. The advantage of a Lexan model is that it can be buckled without sustaining damage, thus allowing repeated buckling experiments to be performed. Correlation studies were carried out using NASTRAN finite element and BOSOR finite difference models. Buckling and frequency data showed good agreement between analysis and experiment. Pressure–vibration interaction data were obtained to investigate an experimental procedure for extrapolating the interaction curve to predict the critical buckling load. While it was found that extrapolation of these data always overpredicted the buckling pressure, the data were used to develop a procedure that was successfully applied as stop-test criteria in the prototype test.

Nomenclature

E = modulus of elasticity
F = frequency, Hz
F_N = frequency of the Nth mode, Hz
M = meridional half-waves
N = circumferential full waves
p = pressure, psi
t = shell wall thickness, in.
t^* = isogrid effective shell thickness in prototype, in.
p_{cr} = predicted buckling pressure, psi
p_{exp} = experimental buckling pressure, psi
R = p_{cr}/p_{exp}
γ = buckling correlation factor

Introduction

THE finite element method (FEM) has become the primary tool for design verification of aerospace structures. Large, very complicated FEM models can be rapidly generated with the aid of preprocessors, quickly solved using general-purpose FEM codes, and the results displayed by means of postprocessing software. However, as the size of the models grows and the complexity of the structure increases, the possibility of generating flawed results grows rapidly. Sole reliance should not be placed on analytical results when working with very large and very complicated structures.

One alternate method of validating a new design is by testing scale models. Scale models provide a means to assess and validate the analytical tools used on the full-scale structure. In addition, scale models can be used directly to investigate the importance of various design features.

In this study, experiments on buckling under external pressure, vibration, and the interaction of external pressure and vibration were conducted on a scale model of a Titan IV nose cone fairing. The objectives of these experiments were 1) to assess analytical methods used in the prototype design analysis, 2) to experimentally investigate important design features such as the effect of discontinuous rings, and 3) to experimentally investigate a vibration-based diagnostic technique for determining the buckling loads of structures. This diagnostic technique is based on the concept that the natural frequency in the buckle mode shape goes to zero when the critical buckling load is reached. By measuring the modal parameters at various load levels below the critical buckling load, one should, in principle, be able to predict the buckling load by extrapolating the load frequency interaction curve to the zero frequency intercept. Linear, small deflection shell theory predicts a linear interaction curve between the square of the frequency and the mechanical loading (external pressure, axial loading, etc.). Several effects, such as vibration amplitude and shell initial imperfections, actually enter into the problem and cause the interaction curve to deviate significantly from the linear form. In order to predict buckling loads accurately, the nonlinear effects must be understood. Nevertheless, even without a complete understanding of the nonlinear phenomena, vibration-based stop-test criteria can be developed and applied to proof tests of externally loaded shell structures. The development of this technique as a test diagnostic should permit the test director to stop large-scale hardware tests if premature buckling is imminent.

Test Model Description

The Titan IV nose cone (the prototype) shown in Fig. 1a is the upper section of the Titan IV fairing configurations shown in Fig. 1b. It consists of a 15/25-deg biconic shell made of three 120-deg isogrid skin sections joined with three explosively driven separation rails. Isogrid is an integrally stiffened construction concept that exhibits isotropic behavior and is composed of an equilateral triangular rib pattern with a thin skin. In the 25-deg cone, the isogrid skins are configured so that no skin splice joints are necessary; however, in the 15-deg cone, two skin panels are required in each trisector. Thus, in the 15-deg cone, three skin splice joints are required in addition to the three separation rails. Each skin splice is located in the middle of each 120-deg section.

When the explosives in the separation rails are detonated, the fairing separates into three trisectors that fall away from the launch vehicle to permit deployment of the payload. As

Presented as Paper 89-1316 at the AIAA 30th Structures, Structual Dynamics, and Materials Conference, Mobile, AL, April 3–7, 1989; received Sept. 12, 1990; revision received Jan. 17, 1991; accepted for publication Jan. 25, 1991.

*Technical Specialist, 5301 Bolsa Avenue.
†Senior Manager, Material & Process Engineering. Senior Member AIAA.
‡Manager, Advanced Structures. Senior Member AIAA.
§Manager, Dynamics Technology.

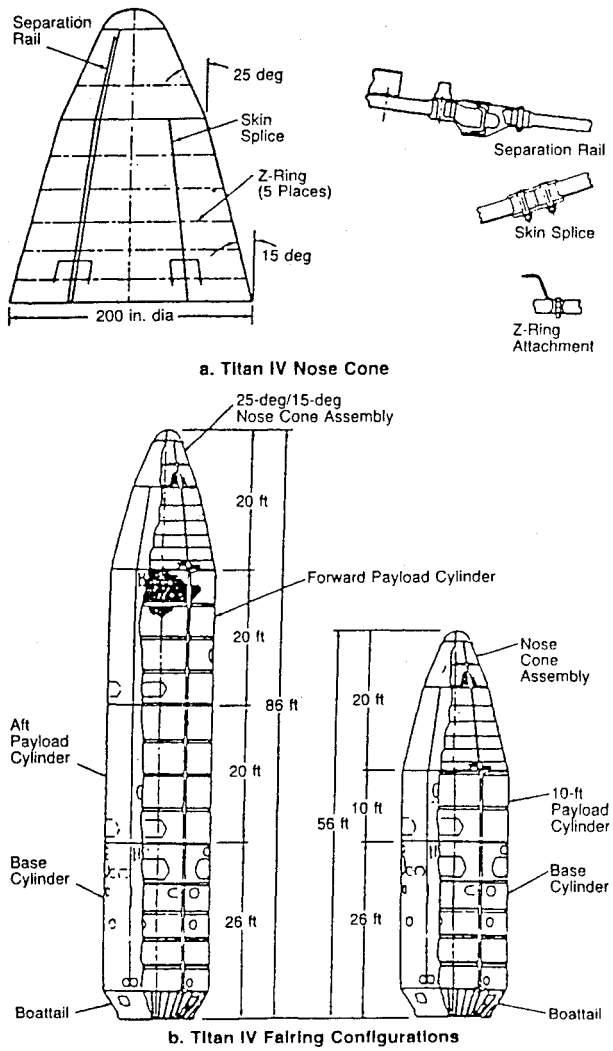

Fig. 1 Titan IV fairing.

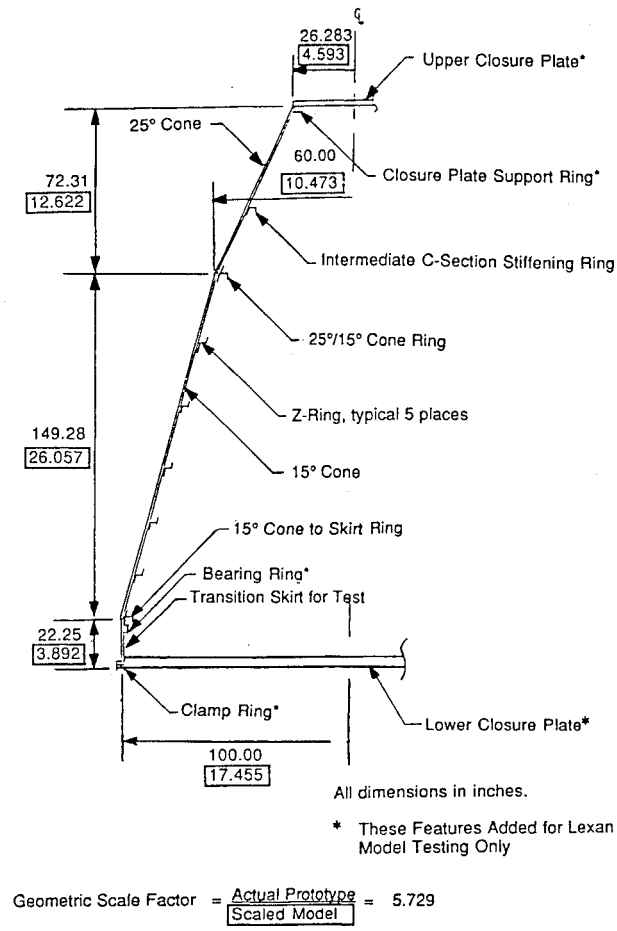

Fig. 2 Schematic of Lexan model.

a consequence of the separation approach, most internal rings are discontinuous at the separation rail locations. The 25-deg cone contains an intermediate C-section stiffening ring and the 15-deg cone contains five Z-section stiffening rings. These rings are attached to the isogrid skin using spacers that connect the ring flange to the isogrid skin pocket. The attachment method results in both in-plane and out-of-plane flexibility. The stiffnesses quantified by subcomponent experiments were utilized in the prototype analysis and design of the scale model.

The scale model was constructed of Lexan (a General Electric brand of polycarbonate plastic). Previous experience with Lexan buckling models has demonstrated that repeatable buckling loads can be obtained from a single model if deformations are restricted in the postbuckled state so as to not yield the material. Key features of the prototype incorporated into the model were flexible discontinuous rings, flexible attachment of the rings to the shell, separation rails, and skin splices. The isogrid skins in each cone of the prototype were modeled as Lexan monocoque skins in the scale model. Since the prototype and model were made of dissimilar materials, the scaling law was based on equating buckling strains (rather than stress) or p_{cr}/E. The scale factor was established by the ratio of isogrid effective thickness in the 15-deg cone ($t^* = 0.516$ in.) to Lexan model thickness ($t = 0.090$ in.) providing a scale factor of 5.73.

A schematic of the model is shown in Fig. 2. The short cylindrical skirt shown at the base of the 15-deg cone modeled the skirt that was used in the prototype test. It provided an interface between the nose cone assembly and the floor of the structural test laboratory and was required to provide a known boundary condition at the nose cone base.

Experiment Description

The model was first tested with continuous Z-section stiffening rings. Buckling experiments were carried out first followed by the modal survey. Once the buckling pressure was known, the pressure levels at which modal data were obtained under load could be selected to provide the best definition of the pressure versus frequency squared interaction curve. Following the experiments conducted on the model with continuous rings, the Z-rings were cut at each simulated separation rail to their setback distances determined by geometric scaling. Approximately 6 deg of arc of each Z-ring were removed at each of these three locations. The buckling and modal survey experiments were then repeated with discontinuous Z-rings. An internal constraint fixture was used during all tests to limit postbuckling deformation and thus minimize potential damage to the Lexan model. The test setup for both buckling and vibration is shown in Fig. 3.

Buckling

A standard laboratory vacuum pump was used to partially evacuate the model. The net external pressure on the model was determined with three pressure transducers. Buckling occurred only in the 15-deg cone of the model as anticipated from pretest analysis conducted on both the model and prototype. In all tests, a meridional mode shape of $M = 1$ corresponding to one longitudinal half-wave was observed in the 15-deg cone. Experimental buckling pressures and circumferential mode shapes are given in Table 1 for both continuous and discontinuous Z-ring stiffening.

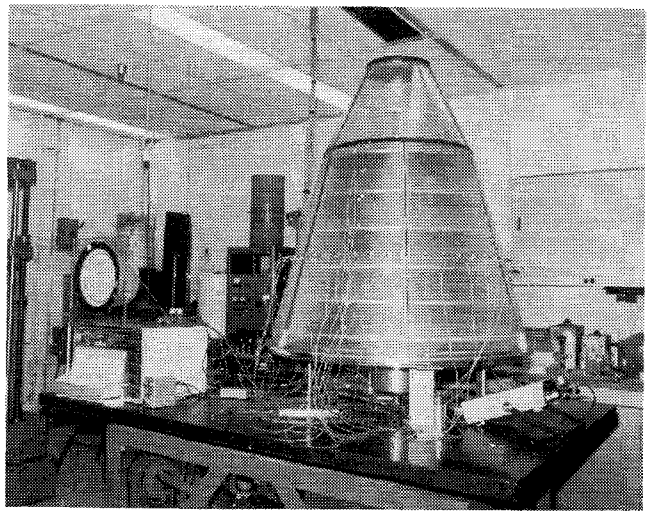

Fig. 3 Test setup.

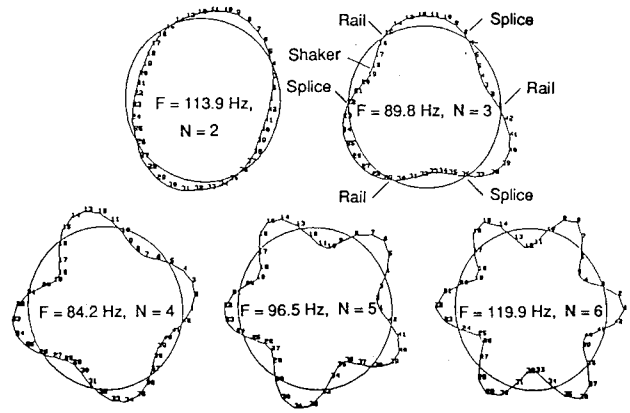

Fig. 4 Experimental frequencies and mode shapes for continuous Z-ring stiffening without pressure.

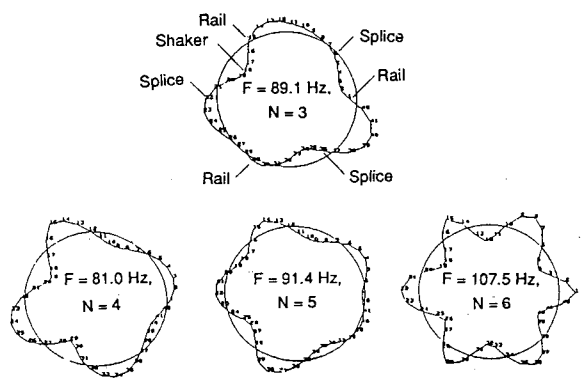

Fig. 5 Experimental frequencies and mode shapes for discontinuous Z-ring stiffening without pressure.

Modal Survey

Forty-two accelerometers were placed at equal distances around the circumference and five were placed at equal meridional distance along the 15-deg cone to determine the shell mode shapes and frequencies. A 4.5-lb force shaker was suspended on an bungee cord and attached to a load cell through a 1/32-in.-diam stinger. A random noise generator provided the input excitation force for the test.

Mode shapes and frequencies were first obtained for the unloaded condition. Frequencies and circumferential mode shapes are given in Table 2 and are shown in Fig. 4 for the continuous Z-ring configuration and in Fig. 5 for the discontinuous Z-ring configuration. Data were then collected at incremental values of the critical buckling pressure. A full set of frequency response functions was collected at each pressure increment.

Analytical Methods and Models

The analytical methods and models applied to the correlation of the Lexan model test results were patterned after their counterparts used in the full-scale nose cone fairing prototype analysis. The purpose of the Lexan model correlation study was to validate the analytical methods and models. The analytical methods used were the structural analysis codes MacNeal-Schwendler (MSC) NASTRAN[1] and BOSOR4.[2]

Two analytical models used with these methods were the NASTRAN model and the BOSOR model. These analysis models used measured model dimensions and measured Lexan material properties. The models were used to determine buckling behavior, vibration behavior, and the interaction between vibration behavior and external pressure loading.

NASTRAN Model

MSC/NASTRAN is a large-scale, general-purpose computer code that performs static, dynamic, and heat transfer analysis by the finite element method. The NASTRAN model was used to determine the shell buckling loads and associated mode shapes, and the natural frequencies and mode shapes for the unloaded shell. Interactions between external loading and frequencies were not determined with the NASTRAN model since the version of NASTRAN used in this study did not permit this type of analysis when the cyclic symmetry option was selected.

The NASTRAN model used plate elements to model the basic shell structure, the circumferential stiffening rings (Z-rings), the ring-to-shell attachments, the skin splices, and the separation rails. A 60-deg symmetry model of a single trisector was modeled and then turned into a 360-deg model using the cyclic symmetry option. The complete model consisted of 33,042 deg of freedom. NASTRAN solution sequences 77 and 48 were used for cyclic symmetry buckling and normal modes calculations, respectively. The enhanced inverse power method was used for eigenvalue extraction. All NASTRAN calculations were executed on a Cray X-MP computer. Fig. 6 shows the NASTRAN model.

BOSOR Model

BOSOR4 performs stress, stability, and vibration analysis of complex branched shells of revolution by the finite difference method. The BOSOR model (Fig. 7) was used to predict

Table 1 Experimental buckling pressures and mode shapes

Z-ring configuration	Buckling pressure, psi	Circumferential mode shape, $N(M = 1)$
Continuous	2.45	5
Discontinuous	1.72	6

Table 2 Experimental frequencies and mode shapes

Z-ring configuration	Frequency, Hz	Circumferential mode shape, $N(M = 1)$
Continuous	113.9	2
	89.8	3
	84.2	4
	96.5	5
	119.9	6
Discontinuous	89.1	3
	81.0	4
	91.4	5
	107.5	6

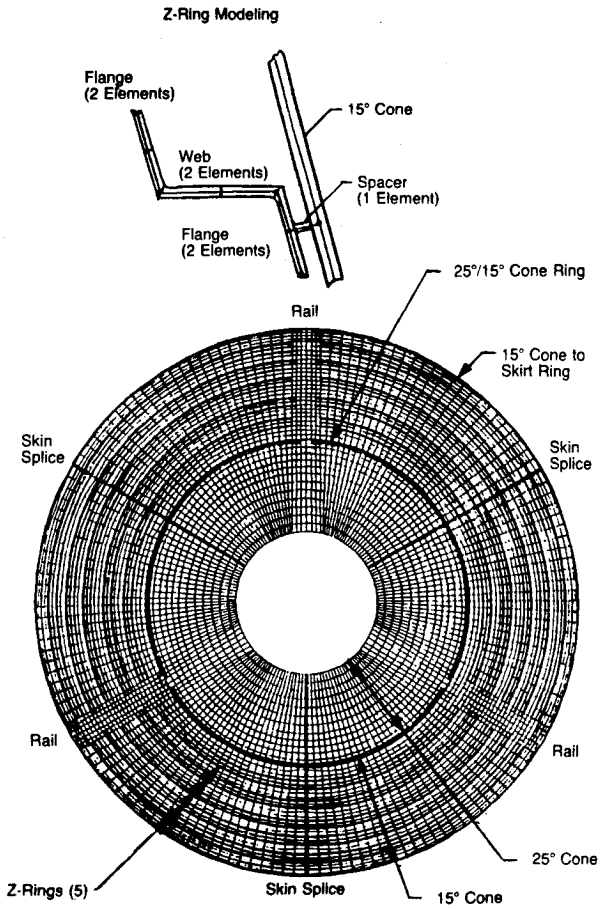

Fig. 6 NASTRAN cyclic symmetry model.

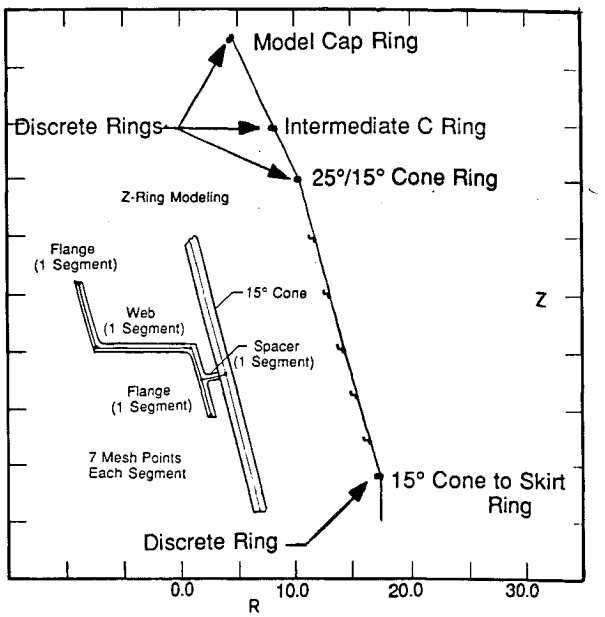

Fig. 7 BOSOR flexible Z-ring model.

buckling loads, natural frequencies, and the interaction between applied loading and natural frequencies. The model included the basic shell structure, the circumferential stiffening rings (Z-rings), and the ring-to-shell attachments. Two versions of the model were made; one modeled the Z-rings as discrete members using the areas of inertias of the Z-rings. The other version modeled the Z-rings and their attachment as flexible members by using model segments to represent the rings and their attachment as branched shells. The separation rails and the skin splices could not be incorporated into the model as a result of the axisymmetric restrictions of BOSOR. Likewise, the discontinuous nature of the Z-rings was not modeled. The BOSOR models had 356 and 2804 deg of freedom for the discrete Z-ring model and the branch shell Z-ring model, respectively. BOSOR was executed on a CDC Cyber 175 computer.

Buckling and Frequency Correlation

Tests were conducted on the model with continuous Z-rings prior to conducting tests with discontinuous Z-rings. This provided the opportunity to correlate a less complex configuration and to also directly compare experimental data, and thus directly assess the effect of discontinuous rings. Prior to testing, the NASTRAN model and the BOSOR model were used to predict buckling pressures and natural frequencies.

Continuous Z-Rings

Table 3 lists both the experimental data and analytical predictions for buckling and frequency. In each column a pressure or frequency value is given along with its corresponding mode number. The mode number describes the number of full sinusoidal circumferential waves (N) into which the shell deforms at the particular buckling load or resonant frequency. All data correspond to one longitudinal half-wave ($M = 1$). As can be seen from the experimental values in the table, the analytical predictions for buckling predicted the $N = 5$ mode to be critical. The experiment verified these predictions.

Table 3 Correlation for continuous Z-ring stiffened shell

	Analysis model								
	NASTRAN			BOSOR					
Experiment	Flexible Z-rings and attachment			Flexible Z-rings and attachment			Discrete rings rigid attachment		
Buckling pressure (p), psi, mode shape (N), and ratio of analysis to experiment (R)									
p	N	p	N	R	p	N	R	p	N	R
2.45	5	2.95	5	1.20	2.51	5	1.02	3.15	5	1.29
Vibration frequency (F), Hz in buckle mode shape (N) and ratio of analysis to experiment (R)									
F_N	N	F_N	R		F_N	R		F_N	R	
113.9	2	88.4	0.78		108.1	0.95		108.5	0.95	
89.8	3	97.7	1.08		98.7	1.10		100.8	1.12	
84.2	4	93.4	1.10		89.4	1.06		95.8	1.14	
96.5	5	106.4	1.10		100.9	1.05		113.8	1.18	
119.9	6	N/A	—		126.2	1.05		146.0	1.22	

The NASTRAN model overpredicted the experimental buckling pressure by 20%. The overprediction is believed to be due to the modeling of the Z-ring flexibility. A mesh convergence study conducted on a single Z-ring after the correlation study was completed suggests that modeling the Z-ring in NASTRAN with two elements representing each flange and the web does not provide the necessary flexibility for the ring. The BOSOR model used seven finite difference mesh points to model each element of the Z-ring. Modeling the Z-rings as discrete and the ring-to-shell attachment in BOSOR as rigid produces a buckling pressure of 3.15 psi which agrees closely to the NASTRAN model prediction of 2.94 psi. This further suggests that Z-ring flexibility was not adequately represented in the NASTRAN model.

The BOSOR model, which is axisymmetric and therefore does not account for asymmetries due to rails and skin splices, overpredicted the experimental buckling pressure by 2%. These results are based on predictions of the BOSOR model that modeled the Z-rings and their attachment as branched shells and thus account for ring and attachment flexibility. When the rings are modeled by their areas and inertias, BOSOR overpredicted by 29%.

Figure 8 further illustrates the importance of correctly accounting for ring and attachment flexibility. In this figure, the predicted buckling pressure as a function of circumferential wave number shows both the general instability and local (between Z-ring) shell instability branches of the stability curve. Modeling the ring and standoff flexibilities produces a lower general instability prediction and better correlation with test. It also reduces the predicted buckling pressure for buckling between Z-rings because the ring flexibility affects the boundary conditions of the shell between Z-rings.

The NASTRAN and BOSOR model results are correlated

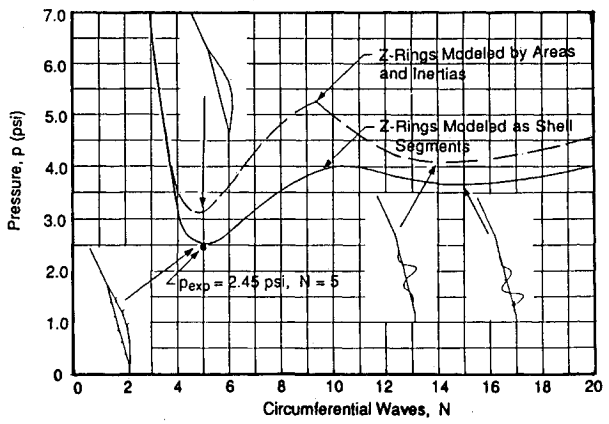

Fig. 8 BOSOR model buckling predictions for continuous Z-rings modeled as discrete rings and as flexible rings.

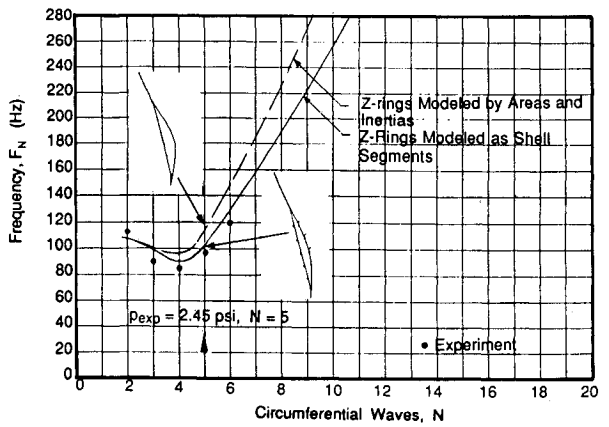

Fig. 9 BOSOR model frequency predictions for continuous Z-rings modeled as discrete rings and as flexible rings.

Table 4 Correlation for discontinuous Z-ring stiffened shell

Experiment		NASTRAN analysis model flexible Z-rings and attachment			
Buckling pressure (p), psi, mode shape (N), and ratio of analysis to experiment (R)					
p	N	p	N		R
1.72	6	2.09	6	Asymmetric at rail	1.22
		2.30	6	Symmetric at rail	—
		2.08	5	—	1.21
		2.33	5	—	—
Vibration frequency (F), Hz, in buckle mode shape (N) and ratio of analysis to experiment (R)					
F_N	N	F_N	N		R
89.1	3	97.3	3	Asymmetric at rail	1.09
N/A		98.5	3	Symmetric at rail	—
81.0	4	85.9	4	Symmetric at rail	1.06
N/A		90.2	4	Asymmetric at rail	—
91.4	5	97.4	5	—	1.07
107.5	6	115.9	6	Symmetric at rail	1.08
N/A	6	121.2	6	Asymmetric at rail	—

to the frequency data in Table 3. The NASTRAN predicted frequencies are higher than those measured by approximately 10%. The discrepancy in frequency is less than for buckling.

The BOSOR model incorporates ring and attachment flexibilities agrees well with experimental data. Measured and predicted frequencies in the buckle mode shape ($N = 5$) agree within 10%. Recall that this axisymmetric model neglects the effects of rails and skin splices. As shown in Fig. 9, including the ring and attachment flexibility in the model produces better correlation than when the Z-rings are modeled as areas and inertias.

Discontinuous Z-Ring Stiffened Shell Correlation

The highest fidelity experimental simulation of the prototype nose cone was achieved by modifying the Lexan configuration described in the previous section; approximately 6 deg of arc of each Z-ring were removed at each of three rail locations. The discontinuous rings prevented the use of the BOSOR code due to the nonaxisymmetric nature of this configuration. Table 4 gives the experimental data and the NASTRAN model predictions for the buckling load. The NASTRAN model overpredicted the experimental buckling pressure by 21%.

The NASTRAN model predicted the $N = 5$ mode to be critical, while the test model demonstrated an $N = 6$ mode. The eigenvalues predicted by NASTRAN for the two modes are very close, yet significantly greater than the test value. Because of the pronounced asymmetry of this shell configuration, two mode shapes are predicted for the global $N = 6$ waveform (see Fig. 10). These correspond to circumferential buckle mode shapes that are symmetric and asymmetric with respect to the rails. It was not possible to distinguish between the symmetric and asymmetric mode shapes in the buckling experiment because both shapes have maximum displacement amplitude at or near the rail and large displacements were prevented by the internal support tree.

Frequency data are correlated in Table 4. The NASTRAN model predictions are high by 9%. Figure 11 shows the frequency mode shapes predicted by the NASTRAN model. Two frequency mode shapes were predicted for the global $N = 6$ mode just as was found for buckling. Test data (Fig. 5) show the lowest frequencies correspond to the symmetric mode.

Correlation Summary

The degree of correlation achieved does not differ between continuous and discontinuous Z-ring configurations. As would be anticipated, the frequency data show better correlation than do the buckling data.

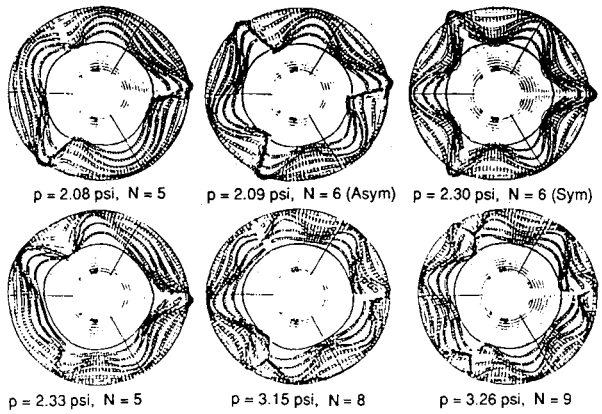

Fig. 10 NASTRAN model buckling eigenvectors for discontinuous Z-ring stiffened shell.

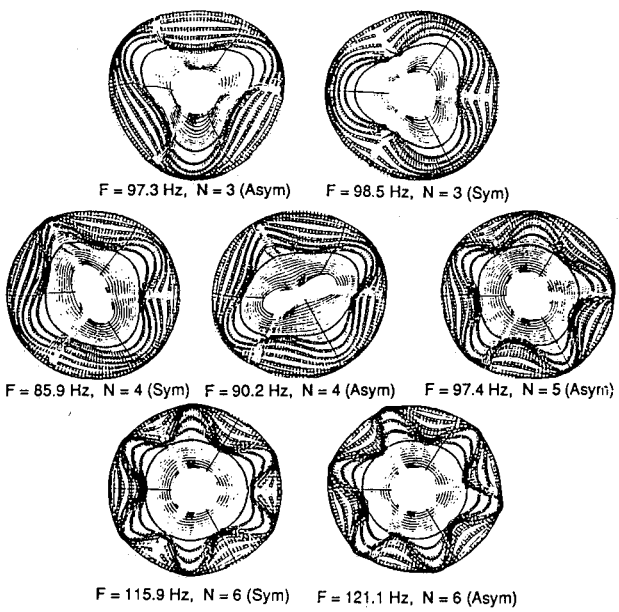

Fig. 11 NASTRAN model frequency eigenvectors for discontinuous Z-ring stiffened shell.

Frequency–Pressure Interaction

Frequency data as a function of external pressure were obtained to determine the feasibility of developing a vibration diagnostic technique for prediction of buckling loads during prototype testing. Shell buckling is usually so catastrophic in the prototype that repair of buckled hardware for retest is impossible. Having an effective diagnostic technique that can be used to monitor large-scale buckling tests provides the test conductor with the capability for stopping a test before premature failure.

Experimental Data and Theoretical Considerations

Small deflection theory predicts a linear interaction curve between the square of the frequency and external pressure loading. The interaction test data obtained for the continuous Z-ring stiffened shell[3] are presented by plotting frequency squared as the ordinate and external pressure as the abscissa as shown in Fig. 12.

Referring to the continuous Z-ring data (Fig. 12), we note that except for the buckle mode shape, $N = 5$, nearly all data plot as straight lines with differing slopes. For $N = 5$, the first three data points also plot a straight line, and if this line is extrapolated to the zero frequency intercept (i.e., the buckling load), the projected pressure overestimates the experimental value by 9%. The general character of the data for the buckle mode shape is that they become quite nonlinear at approximately 80% of the actual buckle pressure; a nonlinear effect most likely produced by the effect of initial imperfections. This occurs at approximately one-half the unloaded frequency (one-fourth of the frequency squared) in the buckle mode shape.

It is important to note that the most important frequency to track during an experiment is the one in the buckle mode shape. Figure 12 shows experimental results for mode shapes $N = 3$, 4, and 6 as well as the buckle mode shape $N = 5$. The unloaded frequencies for $N = 3$ and 4 are lower than for $N = 5$, but as external pressure is applied the curves cross and $N = 5$ results in the lowest frequency near buckling.

The data for the continuous Z-ring configuration are shown correlated with the BOSOR model in Fig. 13. The NASTRAN cyclic symmetry model, as stated above, was only capable of predicting the endpoints of the interaction curve; namely, the buckling load ($F = 0.0$ Hz) and the unloaded vibration frequency ($p = 0.0$ psi).

The BOSOR analysis model predicted a linear interaction between the square of the frequency and the external pressure. The test data, however, are linear only as long as the applied load remains below approximately 80% of the critical buckling load. Above these load values, the interaction curve very rapidly rolls away from the linear interaction and intercepts the pressure axis below the predicted theoretical buckling pressure. This effect has been tentatively attributed to the presence of initial imperfections in the shell geometry. In experimental buckling of shells it is generally accepted that all shells have some initial imperfections and that the presence of imperfections reduces the buckling load. Consequently, using only natural frequencies taken at low load values and then extrapolating a straight line function to determine the zero frequency intercept (buckling load) is unconservative,

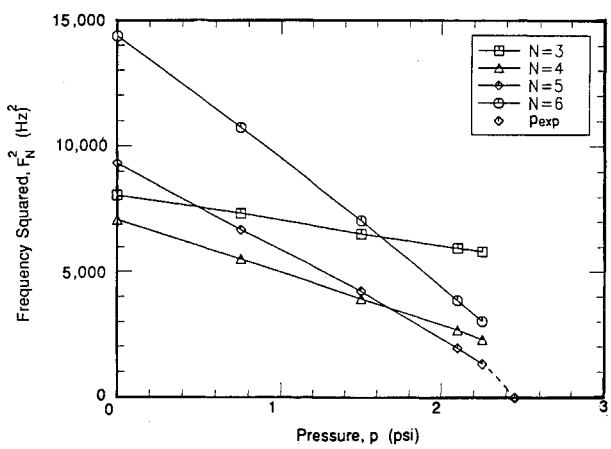

Fig. 12 Experimental pressure–frequency interaction curve for continuous Z-ring stiffening.

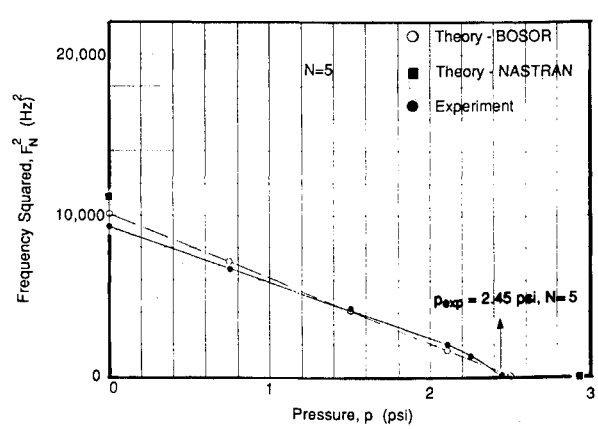

Fig. 13 Pressure–frequency interaction for continuous Z-ring stiffening.

because the nonlinear effect of initial imperfections is greatest near the buckling load.

In addition to rapid roll-off at pressures approaching the buckling load, a second difference between the analytical predictions and experimental results is the disparity in the overall slopes of the two curves. As the load value increases, the interaction of the load with the structure tends to reduce the effective stiffness of the structure. This stiffness change comes into play in the analysis through a term referred to as the differential stiffness. The experimental data are not reduced in frequency as rapidly as the analysis predicts, making the shell appear to be stiffer than modeled.

The "stiffening" effect demonstrated in the test data is most likely a result of the level of excitation used in the vibration testing. Although the analytical techniques are based on the assumption that the vibration amplitude is infinitesimally small, the actual amplitude violates this assumption. Both the vibration amplitude stiffening effect and the initial imperfection-induced roll-off lead to an overestimate of the shell's buckling capability. For this particular case, extrapolating the frequencies taken at low load levels to the zero frequency intercept would result in an unconservative buckling prediction.

Pressure–frequency data obtained from the configuration with discontinuous Z-rings are shown in Fig. 14. Note that because of the pronounced asymmetry of this shell configuration, two mode shapes are obtained for the global $N = 5$ and $N = 6$ waveforms. These correspond to buckle and frequency mode shapes that are symmetric and asymmetric with respect to the rails.

Figure 15 shows the test data $N = 6$ plotted along with the NASTRAN endpoints. Since no BOSOR interaction analysis was available, the NASTRAN endpoints have been connected in a linear fashion to approximate the interaction function. These straight lines cross each other. NASTRAN predicted the $N = 6$ asymmetric mode to give a lower buckling pressure than the $N = 6$ symmetric mode. As mentioned before, it was not possible to distinguish between the symmetric and asymmetric mode shapes in the buckling experiment because both shapes have maximum displacement amplitude at or near the rail and the presence of the internal support tree prevents large displacements. The discontinuous Z-ring configuration displayed a more severe roll-off in frequency near buckling than the configuration with continuous Z-rings.

Vibration Diagnostic Technique for External Pressure Loading

Although linear extrapolation of the frequency squared versus pressure data overpredicted the critical pressure in all of the Lexan model tests, a study of the data indicated that stop-test criteria for prototype testing can be established. The Lexan model data indicated that the unpredictable nonlinear behavior of the interaction curve occurred at a frequency in the

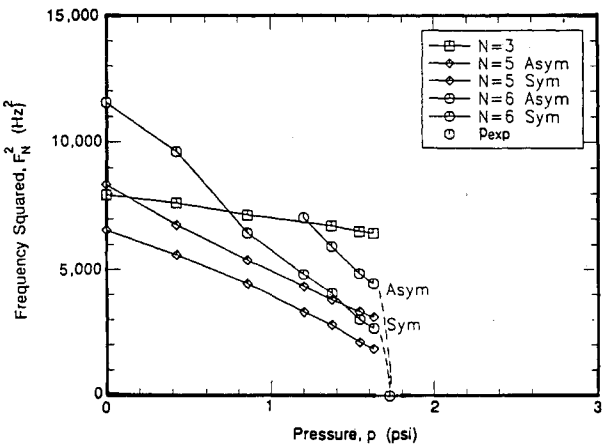

Fig. 14 Experimental pressure–frequency interaction curve for discontinuous Z-ring stiffening.

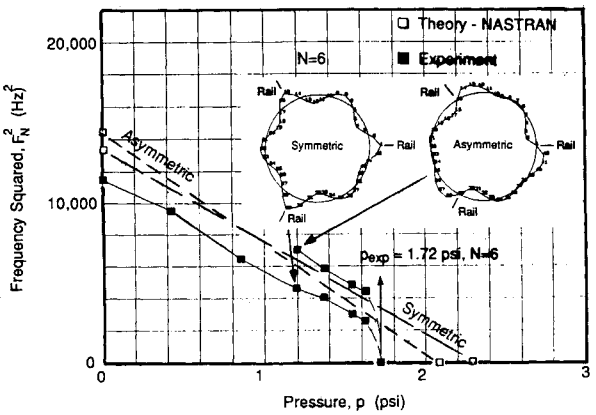

Fig. 15 Pressure–frequency interaction for discontinuous Z-ring stiffening.

buckle mode shape of approximately one-half its free vibration value. Based on this observation, suitable criteria were developed to provide guidance during proof testing of externally pressurized buckling critical shells.

The criteria developed consisted of 1) a trend line, 2) a stop-test criteria, and 3) a load-step selector. The trend line is constructed by connecting points representing the unloaded shell vibration frequency ($p = 0.0$) in the buckle mode shape F_{N0}^2, and 1/4 F_{N0}^2 at the anticipated buckling pressure. This anticipated buckling pressure is determined by reducing the theoretical predicted buckling pressure by the appropriate correlation factor γ. The recommended value of γ from Ref. 4 is 0.75. The resulting trend line is given by

$$\left(\frac{F_{Np}}{F_{N0}}\right)^2 = 1.0 - \frac{3}{4}\frac{p}{\gamma p_{cr}} \tag{1}$$

where F_{Np} is the frequency in the buckle mode shape at pressure, p. If the buckling mode shape is not certain from calculations, the above criteria can be calculated for all measured modes.

The experimental data will generally follow this line until the frequency has dropped to 50% of the unloaded value. Significant deviation from the trend line, either above or below, indicates a faulty analytical model. The experimental data will deviate from the trend line when the frequency reaches the 50% (25% of frequency squared) value.

While the trend line provides guidance, it is not intended to be used as a stop-test criteria. The stop-test criteria are given by

$$\left(\frac{F_{Np}}{F_{N0}}\right)^2 > 1 - \frac{p}{\gamma p_{cr}} \tag{2}$$

for $0 \le p \le \frac{3}{4}\gamma\, p_{cr}$, and

$$\left(\frac{F_{Np}}{F_{N0}}\right)^2 > \frac{1}{4} \tag{3}$$

for $p > \frac{3}{4}\gamma\, p_{cr}$

These criteria define an absolute lower bound for all measurements. If any measurement point falls below this line, the test should be immediately stopped.

Both the trend line and the stop-test criteria were developed to reflect the rapid frequency roll-off seen in the Lexan model results. For the Lexan model, this imperfection-induced effect occurred at approximately 50% of F_{N0}. However, there is no assurance that the roll-off will occur at the same frequency for all shells loaded by external pressure, or for other types

of loading. Consequently, one other guideline was developed. By using the frequency values of the two most recent measurements, an estimate of the buckling load can be made. One-tenth the difference between the estimated buckling load and the current load value is then used as the increment for the next load step. At the ith load step (p_i) the estimated buckling pressure is

$$p_{\text{est}} = \frac{p_i F^4_{N_{pi-1}} - p_{i-1} F^4_{N_{pi}}}{F^4_{N_{pi-1}} - F^4_{N_{pi}}}. \tag{4}$$

The above equation is for a parabola whose axis is the abscissa and which passes through the last two data points.

Similar criteria were successfully applied to the Titan fairing prototype test which utilized the vibration diagnostic technique to alert the test director if general instability failure were imminent. At each load step the structure was excited by a small shaker while the pressure was held constant.

Observations and Conclusions

Even though the discontinuous rings had only 1.67% of their circumference removed at each separation rail, the buckling load was reduced by 30% over the continuous ring results; frequencies were reduced by 5–10%. Modeling the ring and standoff flexibilities produces a 29% reduction over modeling inertias and areas. The rails and skin splice make a minor contribution to the buckling pressure.

The large data base for the Lexan model provides a means for evaluating frequency response as a diagnostic technique. The simplest of these and the least expensive is the modal survey without load. The data indicate that the frequencies are not as sensitive to design features as is buckling beahvior. The load–frequency interaction technique results in an overestimate of the buckling pressure when the test data are extrapolated to zero frequency. This approach thus results in a unconservative estimate of buckling. However, the data can be used to establish a stop-test criteria. This provides a means of monitoring buckling experiments and allows the test conductor to stop large-scale buckling tests before premature failure occurs. As such, this technique may provide a major advance in the test procedure for monitoring large-scale experiments.

Acknowledgments

The authors wish to thank J. T. Hofeditz, T. L. Smith, and J. S. Mills for their contributions.

References

[1]"MSC/NASTRAN User's Manual—Version 65," MacNeal-Schwendler Corp., Nov. 1985.

[2]Bushnell, D., "Stress, Stability and Vibration of Complex Branch Shells of Revolution, Analysis and User's Manual for BOSOR 4," Lockheed Missile and Space Co., Report LMSC-D243605, March 1971.

[3]Powers, D. R., and Driskill, P. H., "The Use of Modal Parameters in the Prediction of Buckling of Externally Pressurized Shells: Part 2. Experiment Description," *Proceedings of the 7th International Modal Analysis Conference,* Jan. 1989.

[4]"Buckling of Thin-Walled Truncated Cones," NASA SP 8019, Sept. 1968.